LANGMUIR

pubs.acs.org/Langmuir Article

Experimental Investigation of Dropwise Condensation Shedding by Shearing Airflow in Microgravity Using Different Surface Coatings

Milad Shakeri Bonab, Christoph Minetti, Carlo Saverio Iorio, Dongdong Zhao, Qiu-Sheng Liu, Junfei Ou, Roger Kempers, and Alidad Amirfazli*

Cite This: *Langmuir* 2023, 39, 64−74 Read Online

ACCESS | Metrics & More | Article Recommendations | Supporting Information

ABSTRACT: The shedding kinematics of water droplets in a condensation environment when exposed to aerodynamic forces in microgravity was studied. Understanding the shedding of droplets from a surface is a critical part of the dropwise condensation process for improving heat transfer. Because gravity as a droplet removal technique is not available in space, the use of airflow to shed droplets is considered for condensing heat exchangers in environmental control and life support systems. Surface coatings affect drop adhesion, and here, four different surfaces (PMMA, PS, PTFE, and SHS) and various droplet sizes (80, 60, and 40 μL) were used to understand the above phenomenon. It was found that the critical velocity to shed a droplet in microgravity was up to 8% lower than that in normal gravity. Also, the effect of the droplet size was investigated for both microgravity and normal gravity; the shedding velocity was lower for microgravity, and it decreased as droplet size increased. Increasing the hydrophobicity of the coating decreased the critical velocity for shedding. Finally, the droplet was found to detach from superhydrophobic surfaces in microgravity. The detachment of droplets from the substrate will hamper the condensation process that can produce a larger fresh area; also, detachment of droplets and entrainment in airflow counter the concept of removing moisture from the air in a dehumidification process.

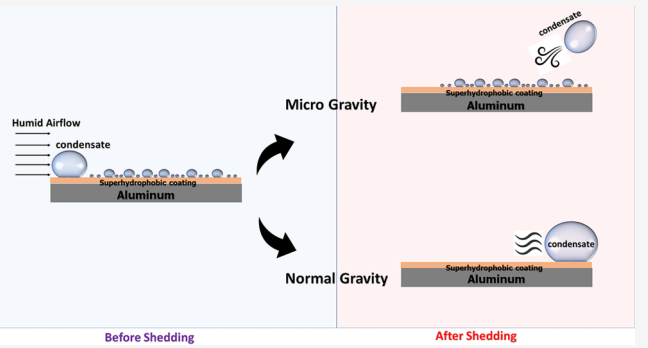

INTRODUCTION

Dropwise condensation (DWC) is a superior mode of heat transfer to its alternative, i.e., filmwise condensation (FWC). The increase in heat transfer coefficient (HTC) can be ten times higher for DWC versus FWC.[1] DWC can improve heat transfer performance in almost all processes that involve a phase change,[2] making its successful application a significant goal for the energy sector[3] (e.g., for power plants, the chemical industry,[2] water desalination,[4] and HVAC systems[5]). This latter point directly relates to the environmental control and life support system (ECLSS) in space vehicles. Also, DWC can be found in other applications related to reduced gravity environments, such as thermal management systems for satellites, power management systems, and wastewater treatment for manned space platforms. The high HTC seen in systems with DWC also means that these systems can be miniaturized, making them lighter. This is essential for space application—an area in which one of the goals for system design is the minimization of a system's weight. However, the condensation phenomenon at the liquid−vapor interface in microgravity (i.e., space applications) is not well understood. Therefore, it is necessary to understand humid air condensation in a microgravity environment.

Shedding (i.e., droplet movement under the effect of an air shear flow) of droplets from a surface is a critical part of the DWC process. The majority of DWC systems take advantage of gravity by causing drops to shed from the surface of a condenser before they grow too large and connect so as to create a film.[6−8] However, for space applications, gravity is not available.[9] A surface energy gradient has been suggested as a way to remove drops;[10,11] however, there can be significant limitations on the distances that drops can be transported on such surfaces. Alternatively, one can take advantage of aerodynamic forces and remove/shed droplets from a surface using a stream of air (note that in ECLSS, an air stream is usually present).[12]

Droplet shedding is mainly determined by adhesion and drag forces. The adhesion force (F_{adh}) is the force that attaches the droplet to the surface; the lateral (i.e., in the plane of the surface) adhesion force $(F_{adh})_{Lateral}$ is a function of contact

Received: July 18, 2022
Revised: December 9, 2022
Published: December 27, 2022

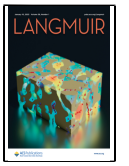

https://doi.org/10.1021/acs.langmuir.2c01898
Langmuir 2023, 39, 64−74

angle (θ), surface tension (σ), and the wetting length (L_w) of the droplet.[13] When a droplet is exposed to a shear flow, the shape of the droplet deforms in such a way that the upstream contact angle (θ_{min}) decreases, and the downstream contact angle (θ_{max}) increases compared with the static contact angle (θ); F_{adh} can be described by the following correlation

$$(F_{adh})_{Lateral} \propto L_w \sigma(\cos\theta_{min} - \cos\theta_{max}) \quad (1)$$

The drag force (F_{drag}) applied on a droplet due to a shear flow can be described by the following correlation

$$F_{drag} \propto 1/2 C_D \rho u_{air}^2 S \quad (2)$$

where C_D is the drag coefficient, ρ is the air density, u_{air} is the free stream velocity, and S is the frontal area (i.e., the area of the droplet that is facing the airflow). When the shear flow is increased over a droplet, the drag force rises accordingly. The opposing lateral adhesion force also increases proportionally. When the airflow is increased to the point of incipient motion of the droplet, the lateral adhesion force is equal to the drag force. The airflow speed associated with the incipient motion is called the critical velocity (u_{cri}). The lateral adhesion force cannot further increase after u_{cri}, and the droplet moves along the surface. The balance of the forces in the horizontal direction is as follows

$$\begin{cases} (F_{adh})_{Lateral} = F_{drag} & \text{up to incipient motion, and at the critical velocity} \\ (F_{adh})_{Lateral} < F_{drag} & \text{after critical velocity} \end{cases} \quad (3)$$

The droplet also experiences vertical adhesion, gravity, and lift (for contact angle > 90°) forces in the vertical direction. When the lift force overcomes the vertical adhesion and gravity forces, the droplet can be detached from the substrate (i.e., entrained in the airflow). The balance of the forces in the vertical direction is as follows

$$\begin{aligned} &(F_{adh})_{vertical} + F_{gravity} \geq F_{lift} && \text{droplet stays attched to the substrate} \\ &(F_{adh})_{vertical} + F_{gravity} < F_{lift} && \text{detachment of droplet} \end{aligned} \quad (4)$$

The use of surface coatings can increase or reduce the force requirements for the shedding by the airflow process. Adhesion of the droplets is a function of surface properties[14] and, indirectly, the condensation period (size of the contact line and change in contact angle[15]). Also, the surface's wettability will significantly affect the size of condensating droplets and the adhesion of droplets onto the surface (Figure 1).[15]

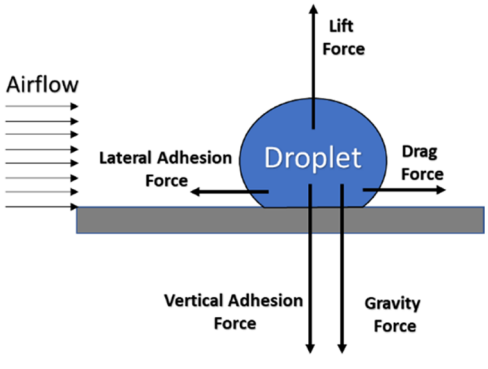

Figure 1. Schematic of a droplet and associated forces due to airflow, wettability, and gravity.

The question of how the adhesion force of droplets can be overcome by aerodynamic forces so they can be shed needs to be answered. There are three possible shedding regimes for the droplet under aero- or hydro-dynamic forces: sliding, deformation−sliding, and deformation−sliding−detachment.[16] The results show that sliding of the condensate improves HTC by providing a fresh area for condensation. One might assume that the detachment of droplets will also offer a fresh area for the condensation cycle; however, when a large droplet detaches, its chance to sweep away tiny droplets downstream, if it was to shed, will be lost (less fresh area available for next cycle of condensation). Currently, it is not clear what the role of surface hydrophobicity in this respect is.

Substrates with lower surface energy provide a higher possibility of shedding due to a lower lateral adhesion force. Therefore, a higher frequency condensation cycle augments the HTC. On the other hand, such substrates have a lower vertical adhesion force and present a higher possibility of droplet detachment, especially in a microgravity environment. Therefore, the main question to answer is whether the vertical adhesion of droplets in the presence of airflow will be sufficiently strong in microgravity conditions to avoid detachment.

In principle, it should be possible to mimic reduced gravity conditions in ground-based applications for deposited droplets; on-ground experiments have demonstrated liftoff of droplets when the droplet density and shearing medium are close.[16] However, in condensation applications, unavoidable differences in the air density and viscosity with water mean that on-ground experiments cannot answer the question of the detachment of droplets. Also, detachment of droplets can be seen if the droplet bursts (i.e., high-speed airflow impulse).[17] However, a burst droplet situation does not address the concern of condensate detachment because it is not a realistic situation for condensation; as such, there is a need for microgravity tests. A parabolic flight (PF) was used to simulate microgravity (weightlessness) to perform experiments under microgravity conditions. In PF, an aircraft flies a parabolic trajectory, providing reduced gravity for up to 23 s.[18]

Only a few studies exist on the influence of microgravity on the shape of droplets. Brutin et al.[19] performed fundamental experiments on sessile drop creation in microgravity. They focused on investigating the drops' interaction with a solid surface (i.e., contact angle) in reduced gravity levels. Three different fluids (de-ionized water, HFE-7100, and FC-72) and two surfaces (aluminum and PTFE) were used in their study. The results show that contact angle behavior depends on the drop diameter and gravity level. They found that the contact angle can be 10° lower for a drop created under normal gravity than the same drop created in microgravity. Drop pressure change through hydrostatic pressure is a possible explanation for the drop contact angle change. Diana et al.[20] characterized droplet shape (contact angle and wetted perimeter) for drops of water and ethanol on aluminum and PTFE substrates under normal gravity and reduced gravity. The wetting diameter and height are related to the surface energy to obtain the lowest free energy shape (spherical cap). The wetting perimeter of the drops was found to be lower in reduced gravity when compared with normal gravity. Also, they discovered that the Young−Laplace equation was not optimal for describing the contact angle for large drops. However, the issue of how reduced gravity can promote droplet liftoff was not addressed in their study.

https://doi.org/10.1021/acs.langmuir.2c01898
Langmuir 2023, 39, 64−74

The current study aims to develop an understanding and evaluation of the shedding of condensate when exposed to airflow (aerodynamic forces) in a microgravity environment. The goal of this study is to determine which coating facilitates the shedding of droplets at a low required air velocity without causing the droplets to lift off the surface. This knowledge will underpin the design of condensers that can work under microgravity conditions and in DWC mode.

METHODS AND MATERIALS

An experimental setup, a mini closed-loop wind tunnel, was designed to investigate the effect of gravity on the shedding of condensate. Condensation took place on a cooled horizontal surface inside the test section. The measurement of parameters such as air velocity, relative humidity (RH), and gravitational acceleration was synchronized to the flow visualization (top and side views of the test section) to characterize gravity's effect on the shedding of droplets. The centroid of the droplet was considered a reference point, and image processing with MATLAB was performed to follow the droplet movement.

Figure 2 shows the line passing through the reference point and the direction of the displacement. The criterion for movement inception

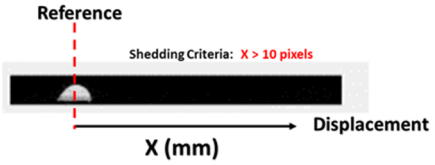

Figure 2. Reference point and the direction of the displacement. The shedding criterion is 10 pix.

(shedding) of the centroid of the droplet was considered to be 10 pix (equivalent to 500 μm; pixel density: 50 ± 0.25 μm/pix).[21−23]

Setup Preparation. The main part of the experimental setup, the wind tunnel, was designed to control RH (ambient—99%), airflow velocity (0−25 m/s), and surface temperature (0−50 °C) to simulate the condensation environment. A PF that was part of the European Space Agency (ESA) 73th PF campaign framework was used to simulate a microgravity environment. The duration of microgravity was approximately 22 s. Due to the time limitation, a single drop was seeded on the condensation surface because condensation is a time-consuming process. Therefore, the droplet injection system was designed to deposit a droplet of a specific volume on the condensing surface. This enabled us to generate an artificial droplet on top of the condensate and to save time.

A schematic diagram and the experimental facility are shown in Figure 3. The test section was 150 mm long with a cross section of 50 mm × 50 mm. The substrate size was 25 mm × 75 mm, located at 20% of the test section's hydraulic diameter after the flow straightener (developing length) to ensure that the nonuniformities of the flow settled.[24] Based on the dimension of the test section (50 mm × 50 mm), maximum velocity before shedding (<5 m/s), and characteristic length for the substrate (75 mm), the entrance length is more than 1 m. The boundary layer thickness at the location of the droplet is less than 1 mm. The bottom surface had a cartridge-like subsystem that enabled the easy replacement of substrates between parabolas in the flight. The aluminum substrates were fitted to grooves in a cartridge. This subsystem was also equipped with a rail fixed to the bottom of the test section (see Supporting Information S.1 for details).

Airflow velocity was controlled by a programmable switching DC power supply (IPS-603, RS Pro), which could change the speed of the fan (MM1865 Series, Mechatronics Inc.). The airflow velocity was measured by a hot-film anemometer (EE75, E+E Elektronik GmbH) with an accuracy of ±0.2 m/s (see details in Supporting Information S.2). The airflow inside the tunnel was humidified using ultrasonic atomizers. The RH was continuously measured and controlled using a programmable humidity controller (HD220, Auber). A closed-loop feedback system controlled the introduction of humidity in the closed-loop tunnel. The control system was capable of maintaining RH in a range between ambient and 99% with an accuracy of ±4% (see details in Supporting Information S.3). The temperature control system was designed to control the temperature of the substrate. The substrate temperature was controlled by a Peltier cell, using closed-loop feedback and a PID algorithm (see details in Supporting Information S.4). Flow visualization was carried out using two cameras (M1280, Genie Nano), which were vertically and horizontally mounted; the field of view was 75 mm (lens: 12 mm/F1.8 VS-1218VM, VS Technology). The captured images were calibrated using a grid array (R1L3S3, THORLABS). The average resolution for the side view was 50 ± 0.25 μm/px, and that for the top view was 65 ± 0.42 μm/px. The droplet injection subsystem consisted of a syringe, a syringe pump (stepper motor), and a linear slider to provide the syringe pump with linear movement (see details in Supporting Information S.5).

A computer powered the hardware via an Arduino board and a joystick (PlayStation). The voltage applied to the fan was controlled by software via an RS232 connection. The Arduino board (Arduino Mega) controlled the syringe pump and collected experimental data: time (for synchronization with the cameras), gravity levels, and power

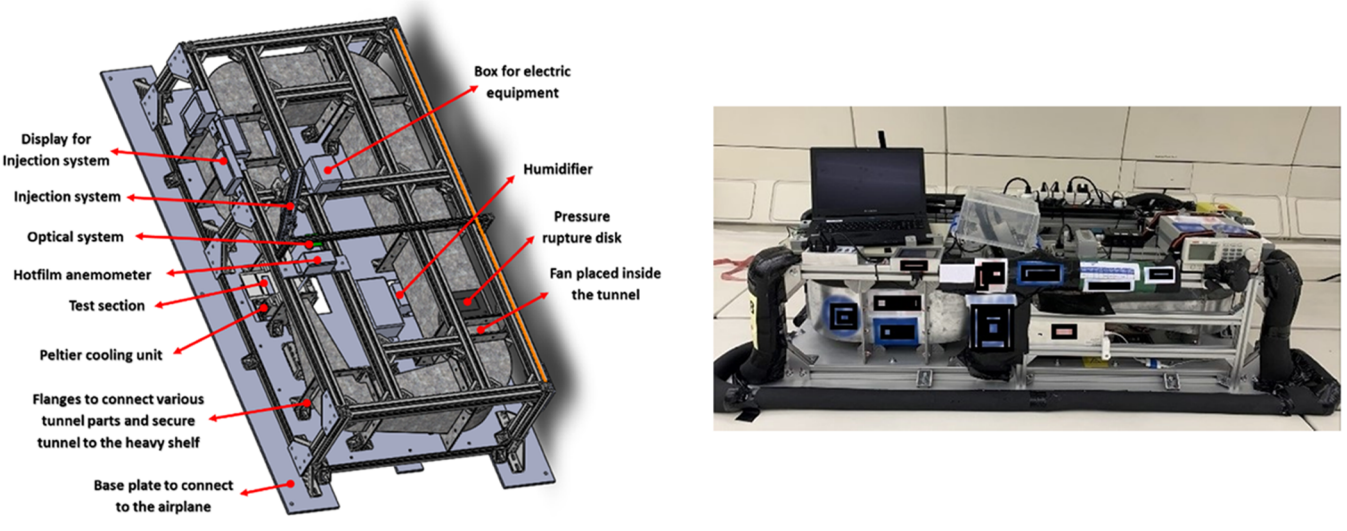

Figure 3. Schematic diagram and the actual experimental facility onboard of the airplane.

https://doi.org/10.1021/acs.langmuir.2c01898
Langmuir 2023, 39, 64−74

for the fan. Commercial software (StreamPix) was used to drive the two cameras. The software overlaid the date and time on the images; these were further synchronized with the gravity levels along the three axes. Finally, the whole experimental setup and operation were controlled by the joystick interface.

Substrate Preparation. To obtain the same morphology, the aluminum substrate was polished with sandpapers (#800, #1200, #2000, #4000, and #8000). Then, roughness measurements were performed using a surface profiler (Dektak 150). The measurements were carried out in the three sections (left, middle, and right) across the substrate length (75 mm) for a length of 55 mm. The process was repeated three times for all substrates, and the average roughness measured was 20 ± 1 nm.

A wide range of contact angles (60−160°) were tested to find the balance between the vertical and horizontal adhesion forces. The aluminum surfaces produced were coated as follows: poly(methyl methacrylate) (PMMA, θ_r = 60 ± 1° and θ_a = 80 ± 1°), polystyrene (PS, θ_r = 70 ± 1° and θ_a = 90 ± 1°), dry PTFE spray (PTFE, θ_r = 80 ± 1° and θ_a = 110 ± 1°), and NeverWet spray (SHS, θ_r > 160° and θ_a > 160°). θ_r is the receding contact angle (i.e., the contact angle measured during the de-wetting process of the substrate), and θ_a is the advancing contact angle (i.e., the contact angle measured during substrate wetting process). Note that the contact angle was measured under normal conditions (i.e., no condensation) and that when condensation occurs, the contact angle is smaller than the values indicated here as expected, see ref 15. A spin-coating technique was used to fabricate PMMA and PS surfaces. However, spraying was used for the PTFE and SHS surfaces. Detailed information on surface fabrication is provided in Table 1.

Table 1. Detailed Information on Surface Fabrication

surface name	method	material and fabrication details
PMMA	spin coat	solution: 2 wt % of PMMA (Aldrich M_w ∼ 120 000) in toluene spin coater speed: 2000 rpm, spin time: 60 s
PS	spin coat	solution: 1 wt % of PS (Aldrich M_w ∼ 35 000) in toluene spin coater speed: 2000 rpm, spin time: 60 s
PTFE	spray coat	material: Dry PTFE spray (ROCOL)
SHS	spray coat	material: NeverWet spray (Rust-Oleum)

RESULTS AND DISCUSSION

We conducted ground-based research as a reference for comparison with the results from reduced gravity. In the ground-based experiments, airspeeds between 3 and 15 m/s caused droplet shedding for all four substrates (no droplet detachment/liftoff). Such airspeeds were necessary to overcome the horizontal adhesion force of a droplet onto the substrate. Microgravity tests were carried out to determine whether these speeds cause droplets to lift off from the surface. Based on our experience from the ground-based experiments,[25] we chose to conduct the tests at a humidity level of 80%, as this would provide a higher rate of condensation and yet would not create fog on the walls of the test section.

Drop Shape. Considering a stationary droplet on a horizontal flat surface, gravity acts downward, perpendicular to the surface (note that a microgravity environment cancels the downward gravity, and this work focuses on the effect of downward gravity on condensation). For small droplets, a spherical cap can be used to approximate the droplet shape (see Figure 4), where R_c is the characteristic length, r is the radius of the contact line, h is the height of the droplet, and θ_c is the contact angle. The force balance at the liquid−air interface determines the equilibrium shape of the droplet. The

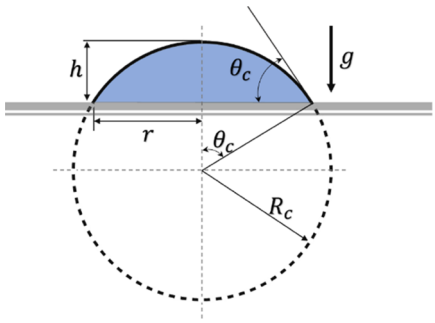

Figure 4. Stationary droplet on a horizontal flat surface. The droplet is modeled as a spherical cap, which is a sphere cut off by the surface, where R_c is the characteristic length, r is the radius of the contact line, h is the height of the droplet, and θ_c is the contact angle. A downward arrow shows the gravity vector g.

Young−Laplace equation expresses the balance due to the pressure difference across the interface by surface tension and gravity forces. Gravity causes hydrostatic pressure inside the droplet. The dimensionless Bond number, $Bo = \frac{\rho g R_c^2}{\gamma}$, determines the strength of gravitational force relative to the surface tension force, where ρ, g, and γ represent the liquid density, gravity acceleration, and surface tension, respectively. In zero gravity (i.e., Bo = 0), hydrostatic pressure becomes zero, and the mean curvature of the droplet stays constant, leading the droplet to have a spherical cap shape; the contact angle (depending on the wetting properties of the substrate) will determine the spherical cap shape for a given drop volume. In the presence of gravity (i.e., Bo is finite), the drop shape deviates from a spherical cap because the hydrostatic pressure is no longer zero.

Volume and characteristic length can be calculated using the equations below for a spherical cap

$$V = \frac{1}{6}\pi h(3r^2 + h^2) \quad R_c = \frac{r^2 + h^2}{2h} \tag{5}$$

The characteristic length is a function of r and h that defines the scale of the physical system. This length is used as an input to predict some system features. So, the volume of the droplet (V), the radius of the contact line (r), and the height of the droplet are normalized as follows

$$\mathcal{R} = \frac{r}{R_c} = \sin\theta_c$$
$$\mathcal{V} = \frac{V}{R_c^3} = (\pi/3)(2 + \cos\theta_c)(1 - \cos\theta_c)^2$$
$$\mathcal{H} = \frac{h}{R_c} \tag{6}$$

Effect of Microgravity on Droplet Geometry. When the droplet is in microgravity, the contact angle and wetting length can change,[19] potentially altering the balance of forces for droplet shedding. Therefore, shape analysis is an essential step to understand the effect of gravity on the shedding behavior of droplets (the primary objective of this study). The shape analysis for the 40 μL size droplet on a PTFE coating is discussed as an example. Figure 5a illustrates the droplet profile in microgravity and normal gravity (ground). For the same volume of 40 μL, the radius of the contact line (wetting length) of the droplet in microgravity is 8% lower (i.e., 0.45

https://doi.org/10.1021/acs.langmuir.2c01898
Langmuir 2023, 39, 64−74

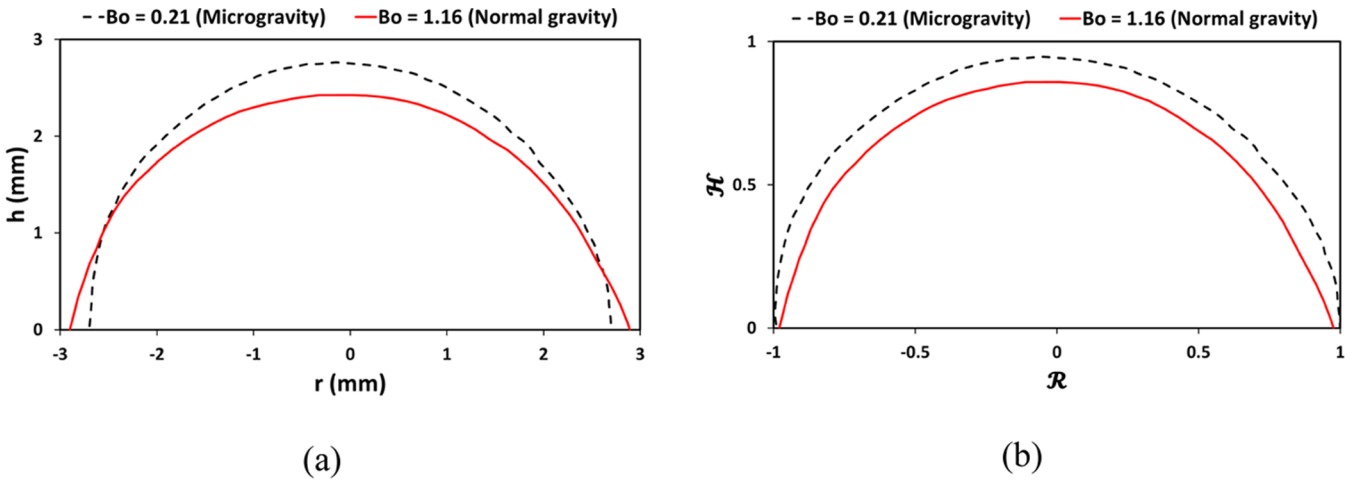

Figure 5. Shape analysis for the 40 μL size droplet on PTFE coating. (a) Droplet profile in microgravity and normal gravity (ground); r is the radius of the contact line, and h is the height of the droplet. (b) Dimensionless plot for the same droplet for the identical condition; $\mathcal{R}$ is the normalized radius of the contact line, and $\mathcal{H}$ is the normalized height of the droplet. The gravity vector, g, is downward.

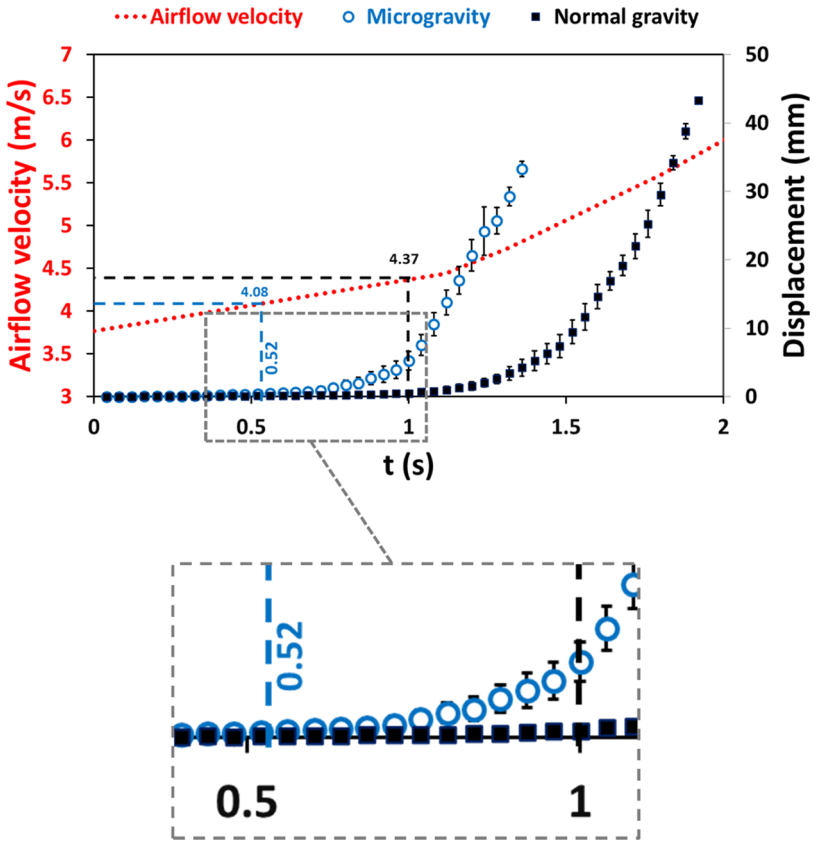

Figure 6. Displacement of the droplet and airflow velocity are superimposed for the same time frame. The coating is PTFE, and the droplet volume is 60 μL. The criterion for movement inception (shedding) of the centroid of the droplet was considered to be 10 pixels. The dotted line is provided to guide the eye.

mm) than in normal gravity. Also, the droplet in the microgravity condition has a contact angle that is 15% higher (i.e., 12°). Note that the droplet was assumed to be axisymmetric in our calculations. Also, the gravity was 0.22g for microgravity at the moment of increasing the airflow velocity. The g-jitter during the microgravity can be found in Supporting Information S.6. As seen in Figure S6, the gravity fluctuation from increasing the velocity to shedding is relatively smooth. Any change in the droplet shape was negligible, according to our observation. By the time gravity fluctuation was more significant, the droplet had been shed, so fluctuation of gravity did not affect the shedding. The adhesion force of the droplet is proportional to the wetting length (L_w) and contact angle (eq 1). A lower wetting length and higher contact angle in microgravity should provide for a lower horizontal adhesion force.

Figure 5b shows the dimensionless plot for the same droplet for an identical condition. The normalized height of a droplet

https://doi.org/10.1021/acs.langmuir.2c01898
Langmuir 2023, 39, 64−74

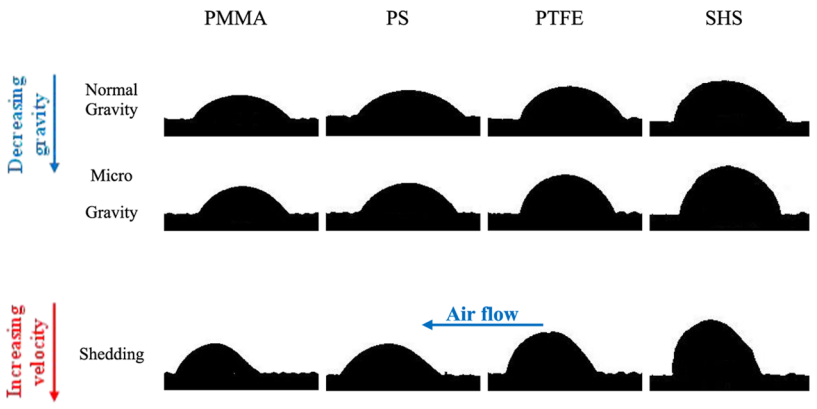

Figure 7. Typical progression of droplet deformation and shedding for different coatings. All droplets are 60 μL in volume. Initially, the axisymmetric droplet (first row, stationary conditions) deforms as the gravity decreases (second row, microgravity condition) and becomes more spherical in reduced gravity than in normal gravity. Then, air velocity increases until critical velocity and runback commences (third row, shedding condition).

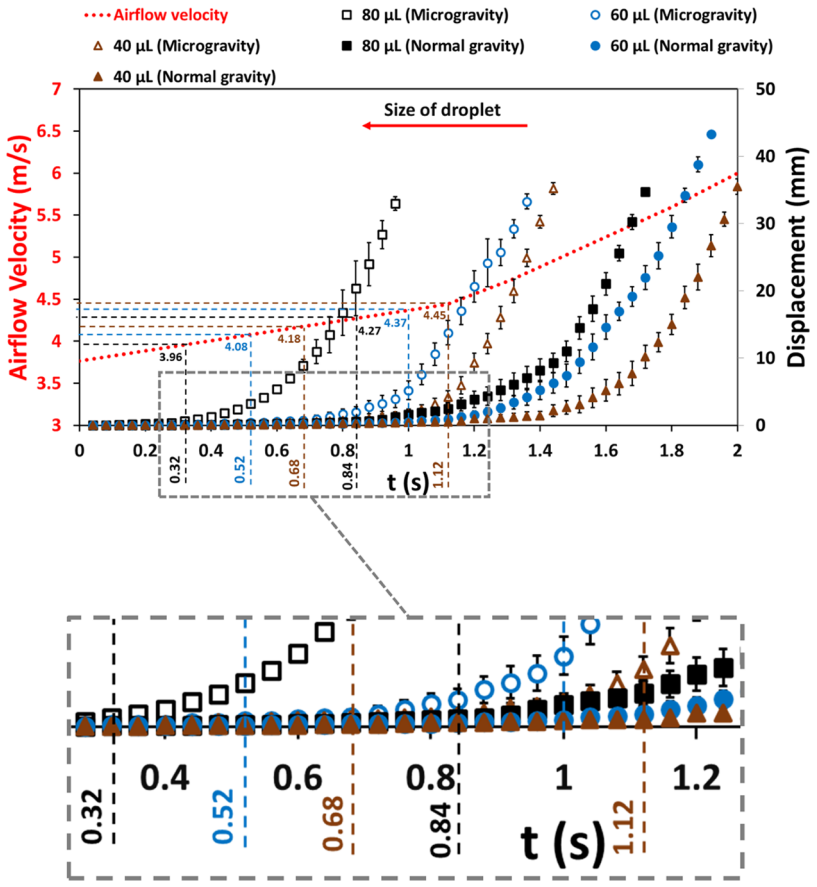

Figure 8. Displacement graph and airflow velocity are superimposed for the same time frame. Different droplet sizes of 40, 60, and 80 μL were tested at microgravity and normal gravity. The surface coating is PTFE. The dotted line is provided to guide the eye. Color plots online.

for microgravity is higher than for normal gravity. The drag force for droplet shedding is proportional to the frontal area (S) of the droplet. Due to the higher normalized height at the same normalized wetting length (the same characteristic length was used for normalization), the drag force is higher for the droplet in the microgravity environment. Note that the shape in Figure 5b does not represent the actual volume of droplets.

Considering all above discussion, the droplet in microgravity is expected to have a lower horizontal adhesion force and undergoes higher drag force compared with normal gravity conditions. Also, as the contact angle increases in microgravity, the lift force increases because of the droplet's shape.[26,27] The total vertical adhesion force also decreases because of the lower wetting length (eq 1). Therefore, the droplet is more vulnerable to detaching from the surface in microgravity than in normal gravity. Note that this section was an example of microgravity's effect on droplet geometry, and similar trends were found for other coatings and droplet sizes.

Shedding Behavior of Droplet in Microgravity. The experiments were conducted at an airflow between 3 and 15

https://doi.org/10.1021/acs.langmuir.2c01898
Langmuir 2023, 39, 64−74

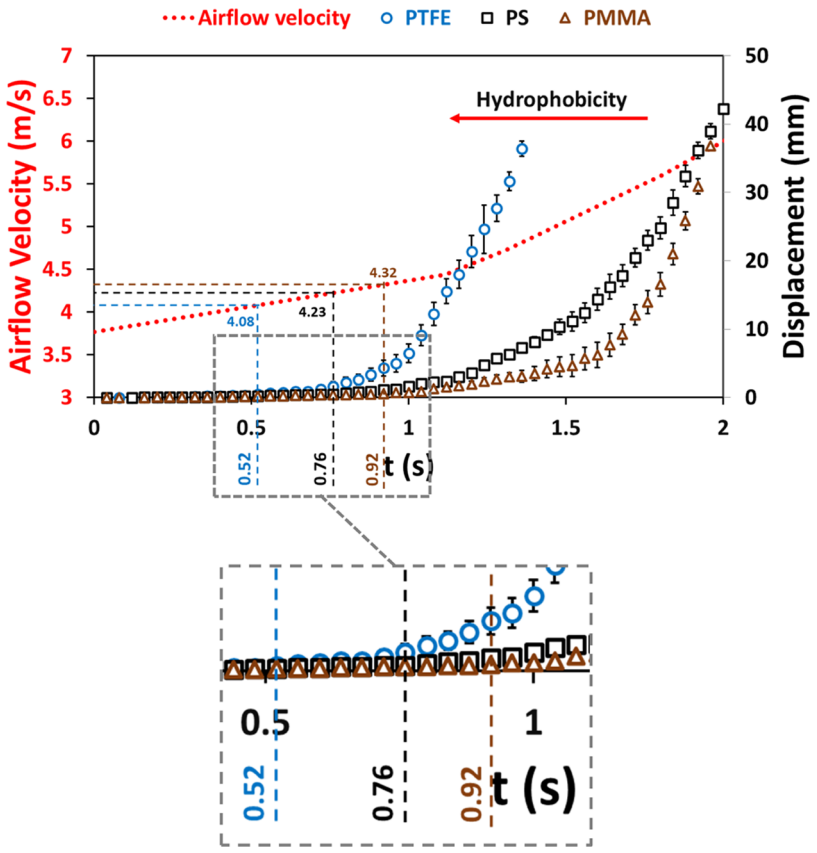

Figure 9. Displacement graph and airflow velocity are superimposed for the same time frame. The different substrate coatings of PMMA, PS, and PTFE were tested at microgravity conditions for the droplet volume of 60 μL. The dotted line is provided to guide the eye.

m/s at 80% RH and 0 °C subcooling. Condensation was allowed to take place for 270−300 s before depositing a droplet. The droplet was deposited 3−5 s before the start of the microgravity phase in PF. Then, 3−5 s after experiencing microgravity, the airflow was increased to 15 m/s. Based on the dimension of the test section (50 mm × 50 mm), maximum velocity before shedding (<5 m/s), and characteristic length for the substrate (75 mm), the entrance length is more than 1 m. The boundary layer thickness at the location of the droplet is less than 1 mm. Shedding behavior for the 60 μL droplet on the PTFE coating is discussed as an example here. The same procedure was performed for the ground experiment (time-wise). Each experiment was repeated four times. Displacement versus time for the microgravity and normal gravity tests are shown in Supporting Information S.7.

Deviations observed for the inception of the droplet movement (i.e., between the repeated tests) were 0.1 and 0.08 s for microgravity and normal gravity, respectively. After shedding started, a higher variation was found for both normal gravity and microgravity tests. A possible explanation is that the seed droplet coalesces with random condensating droplets and may have different sizes and movements in the way of shedding. This deviation was prominent for microgravity results because there was a slight acceleration in the direction of shedding due to the aircraft's movement.

The same approach was used for airflow and droplet movement to achieve identical conditions and to compare microgravity and normal gravity results. The displacement and airflow velocity (i.e., the combined plot from all tests) are superimposed for the same time frame in Figure 6. In microgravity, the droplet shed at a 7% lower airflow velocity compared with that of normal gravity. This confirms our analytical assertions earlier that the droplet experiences a lower horizontal adhesion force and higher drag force in microgravity.

The typical progression of 60 μL droplet deformation and shedding is shown in Figure 7. Each column represents a different coating. It can be seen in Figure 7 that for all droplets, the droplet (first row, stationary conditions) initially deforms as the gravity decreases (second row, microgravity condition). Then, air velocity increases until critical velocity and runback occurs (third row, shedding condition). However, in normal gravity, deformation due to gravity (second row) does not exist, explaining the higher critical velocity in Figure 6. The 40 and 80 μL droplets deformed into similarly trending shapes to those shown in Figure 7, depending on the coating.

Effect of Droplet Size on Shedding. Experiments were conducted for different droplet sizes of 40, 60, and 80 μL to investigate the effect of droplet size on shedding. The same procedure as in the previous section was used. Figure 8 illustrates the results for both microgravity and normal gravity for different droplet sizes. The results clearly show that the shedding velocity is lower for microgravity, and it decreases according to the size of the droplet. Surfaces coated with PMMA, PS, and SHS also show the same trend, with different critical velocities, depending on the coating and droplet size (further data available in ref 28). Critical velocities for 0.5−100 μL droplets are taken from Milne et al.[21] Although the contact angle and interaction of the droplet are different for the substrate in a condensation environment,[15] the trend for

https://doi.org/10.1021/acs.langmuir.2c01898
Langmuir 2023, 39, 64−74

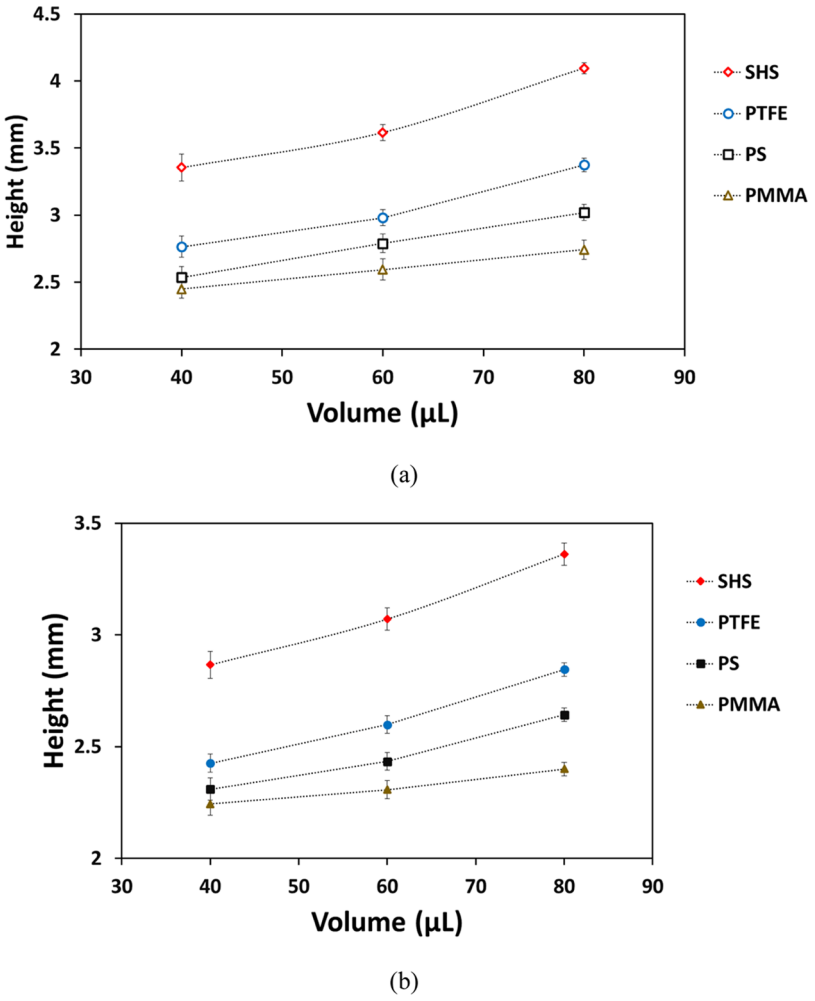

Figure 10. Height versus volume of the droplet. The different substrate coatings of PMMA, PS, PTFE, and SHS were tested under (a) microgravity and (b) normal conditions. The dotted line is provided to guide the eye.

critical velocities is in good agreement with ref 21. In microgravity, a critical velocity improvement (i.e., lower critical velocity) of 8% was found for the droplet size of 80 μL and the surface coated with PTFE.

Effect of Coating on Shedding. The question of how the droplet adhesion force can be overcome by aerodynamic forces in order for shedding to occur can be answered using different coatings; PMMA, PS, PTFE, and SHS used for the same droplet volume of 60 μL are discussed as an example (the same trend exists for 40 and 80 μL droplets; see ref 28). Figure 9 shows the shedding velocities for various coatings. As hydrophobicity increases, the critical shedding velocity decreases. The explanation is that the droplet has lower adhesion forces when hydrophobicity increases. Also, the droplet develops a specific shape for higher hydrophobicity: i.e., higher height for the same volume (Figure 10 shows the height of droplets versus the volume for different substrates). Therefore, the drag force increases when hydrophobicity increases. As a result of lower adhesion and higher drag, a droplet on PTFE coating experiences a lower shedding velocity. Similar behavior can be seen in previous work on PMMA, Teflon, and SHS coatings.[21] Figure 11 shows the critical airflow velocity versus volume for the different coatings.

As discussed before, the critical velocity is determined by the equilibrium between the lateral adhesion force and the drag force. Before shedding, the lateral adhesion force is proportional to the difference between upstream and downstream contact angles. Once the droplet starts moving, its velocity is determined by the dynamic contact angle, droplet shape, and surface condition. As seen in Figure 9, the displacement slope (droplet's movement velocity) for PTFE has a higher slope than that of other substrates (i.e., PMMA and PS) due to its lower lateral dynamic adhesion force. However, as the droplet accumulates more random droplets along its path and grows in size, it is challenging to predict its velocity (i.e., both adhesion and drag forces are changed as the droplet becomes larger).

Detachment of Droplets. As seen in the previous section, increasing hydrophobicity is favorable for decreasing critical velocity. However, this raises a question. By how much can hydrophobicity be increased but still avoid droplet detachment from a surface? To address this concern, we started by examining the most hydrophobic surface, i.e., SHS. It was tested under normal gravity and microgravity, and the results for a 40 μL droplet are discussed as an example. As shown in Figure 12a,b (normal gravity before and after critical velocity, respectively), the shedding path is clear, and the droplet removes tiny droplets along its way as it travels on the surface. Figure 12c,d shows the top view of surfaces under microgravity conditions before and after critical velocity. In Figure 12d, detachment of the droplet is apparent, as the path of cleaned,

https://doi.org/10.1021/acs.langmuir.2c01898
Langmuir 2023, 39, 64−74

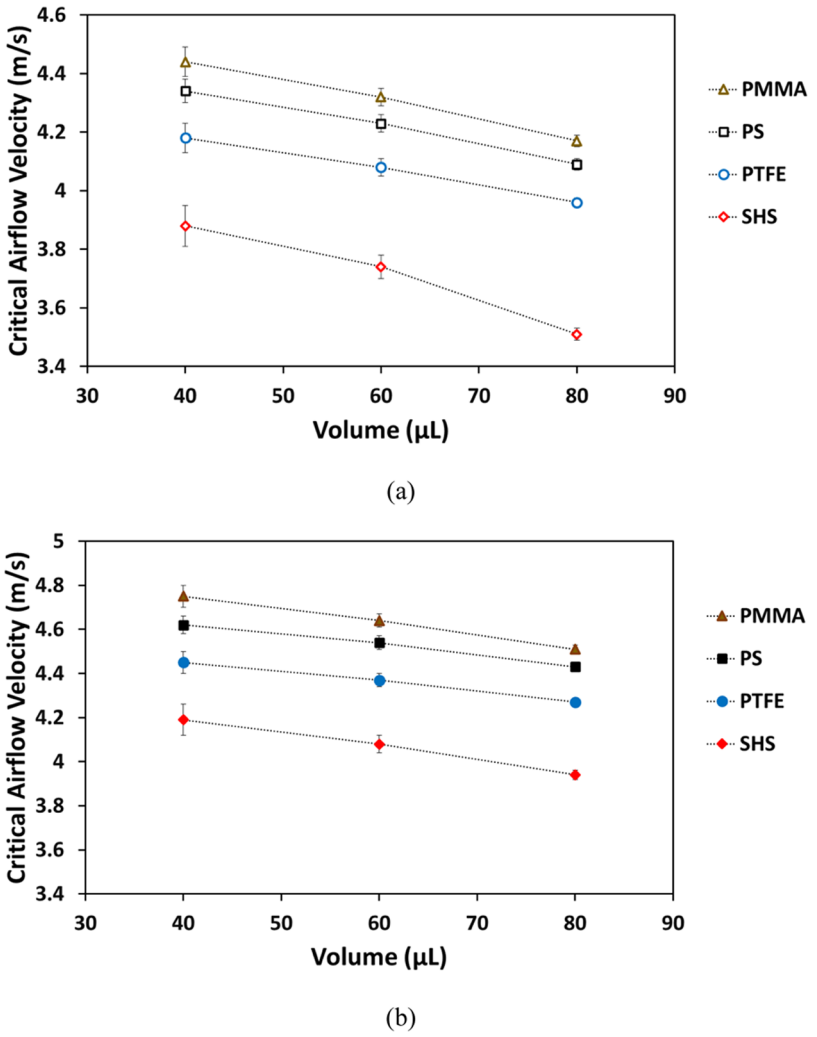

Figure 11. Critical airflow velocity versus volume of the droplet. The different substrate coatings of PMMA, PS, PTFE, and SHS were tested under (a) microgravity and (b) normal condition. The dotted line is provided to guide the eye.

tiny droplets comes to an abrupt end as the seeded droplet detaches from the surface (compare to Figure 12b). The SHS substrate with lower surface energy provides a lower vertical adhesion force (mainly due to the small length of the contact line). In the absence of gravity and considering lower vertical adhesion force, the lift force is prominent and causes the detachment of the droplet; given the shape of the droplet on SHS, the lift force is higher than the case with a low contact angle, e.g., PMMA. As discussed earlier, from a condensation point of view, this is not favorable. Also, previous works showed that the shedding of condensate improves the heat transfer coefficient;[25] however, the shedding process and condensation cycle will not be efficient if the condensate detaches. Droplet detachment was also found for 60 and 80 μL droplet sizes on an SHS in microgravity. As previously discussed, a maximum critical velocity improvement (i.e., lower critical velocity) of 8% was found for the droplet size of 80 μL and the surface coated with PTFE in microgravity. Although an improvement of 12% was found in the critical velocity for the substrate coated with SHS, the droplet detached from the surface, which is not considered as an improvement for the condensation cycle.

It is worth noting that this work is the first of its kind to be done in a microgravity environment. This environment imposes many limitations, such as time, the number of parabolas, and specific safety requirements. As such, it was not possible to try a wide range of substrates to determine the threshold for the hydrophobicity quantitively. It was a preliminary study to see whether the detachment takes place or not. More investigation and tests are required to find the exact threshold of hydrophobicity for droplet detachment.

CONCLUSIONS

Through a simple analytical model constructed, we expected that the shedding velocity for droplets should be lower in microgravity compared to normal gravity. We understood this is so, as in microgravity, the same droplet has lower adhesion (wetting length) and undergoes higher drag force (frontal area). By experimenting under similar conditions on-ground and onboard an aircraft (simulating microgravity conditions), we found that the droplet in microgravity shed at up to 8% lower airflow velocity as compared with normal gravity. We found that increasing hydrophobicity decreases critical velocity in agreement with earlier works. The most novel finding has been the observation of droplet detachment from superhydrophobic surfaces in microgravity. This was explained by the balance of the vertical adhesion force and the aerodynamic lift force the droplet experiences.

https://doi.org/10.1021/acs.langmuir.2c01898
Langmuir 2023, 39, 64−74

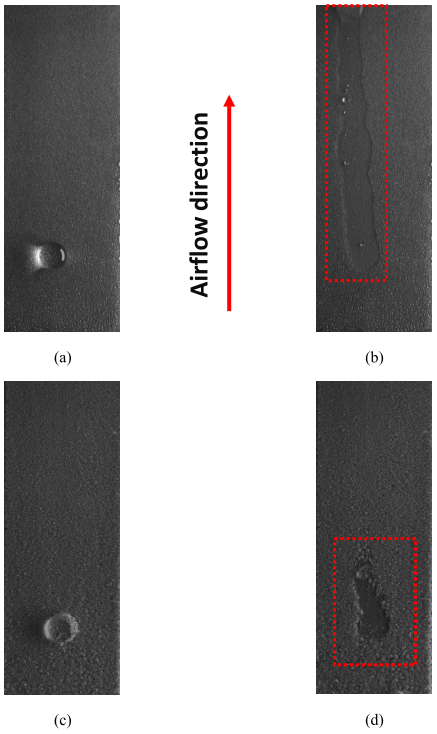

Figure 12. Top view for a 40 μL droplet on the SHS substrate. (a) Normal gravity before critical velocity and (b) after critical velocity. (c) Microgravity before critical velocity. (d) Microgravity after critical velocity.

■ ASSOCIATED CONTENT

Supporting Information

The Supporting Information is available free of charge at https://pubs.acs.org/doi/10.1021/acs.langmuir.2c01898.

Description of the system to change the substrate during the experiments; functional diagram of the velocity, humidity, and temperature control systems; diagram of the droplet injection system; a plot of g-jitter during microgravity; and additional data for experimental repeatability (PDF)

■ AUTHOR INFORMATION

Corresponding Author

Alidad Amirfazli − *Department of Mechanical Engineering, York University, Toronto, Ontario M3J 1P3, Canada;* orcid.org/0000-0002-8391-0493; Email: alidad2@yorku.ca

Authors

Milad Shakeri Bonab − *Department of Mechanical Engineering, York University, Toronto, Ontario M3J 1P3, Canada*

Christoph Minetti − *Service Chimie-Physique, Université Libre de Bruxelles, 1050 Brussels, Belgium*

Carlo Saverio Iorio − *Service Chimie-Physique, Université Libre de Bruxelles, 1050 Brussels, Belgium*

Dongdong Zhao − *Institute of Mechanics, Chinese Academy of Sciences, Beijing 101400, China*

Qiu-Sheng Liu − *Institute of Mechanics, Chinese Academy of Sciences, Beijing 101400, China*

Junfei Ou − *School of Mechanical Engineering, Jiangsu University of Technology, Changzhou 213006, China;* orcid.org/0000-0002-6485-0149

Roger Kempers − *Department of Mechanical Engineering, York University, Toronto, Ontario M3J 1P3, Canada*

Complete contact information is available at: https://pubs.acs.org/10.1021/acs.langmuir.2c01898

Notes

The authors declare no competing financial interest.

■ ACKNOWLEDGMENTS

The project was partially supported by the European Space Agency (ESA) under the MAP program for Condensation and the China Manned Space Agency (CMSA).

■ REFERENCES

(1) Le Fevre, E. J.; Rose, J. W. An Experimental Study of Heat Transfer by Dropwise Condensation. *Int. J. Heat Mass Transfer* **1965**, *8*, 1117−1133.

(2) Ahlers, M.; Buck-Emden, A.; Bart, H. J. Is Dropwise Condensation Feasible? A Review on Surface Modifications for Continuous Dropwise Condensation and a Profitability Analysis. *J. Adv. Res.* **2019**, *16*, 1−13.

(3) Beér, J. M. High Efficiency Electric Power Generation: The Environmental Role. *Prog. Energy Combust. Sci.* **2007**, 107−134.

(4) Parekh, S.; Faridb, M. M.; Selmana, J. R.; Al-Hallaj, S. Solar Desalination with a Humidification-Dehumidification Technique-a Comprehensive Technical Review. *Desalination* **2004**, *160*, 167−186.

(5) Kim, M.-H.; Bullard, C. W. Air-Side Performance of Brazed Aluminum Heat Exchangers under Dehumidifying Conditions. *Int. J. Refrig.* **2002**, *25*, 924−934.

(6) Oh, S.; Revankar, S. T. Experimental and Theoretical Investigation of Film Condensation with Noncondensable Gas. *Int. J. Heat Mass Transfer* **2006**, *49*, 2523−2534.

(7) Ma, X. H.; Zhou, X. D.; Lan, Z.; LI, Y. M.; Zhang, Y. Condensation Heat Transfer Enhancement in the Presence of Non-Condensable Gas Using the Interfacial Effect of Dropwise Condensation. *Int. J. Heat Mass Transfer* **2008**, *51*, 1728−1737.

(8) Huang, J.; Zhang, J.; Wang, L. Review of Vapor Condensation Heat and Mass Transfer in the Presence of Non-Condensable Gas. *Appl. Therm. Eng.* **2015**, 469−484.

(9) Khandekar, S.; Muralidhar, K.*Dropwise Condensation on Inclined Textured Surfaces*; Springer: NYC, USA, 2014; Chapter 4.

(10) Daniel, S.; Chaudhury, M. K.; Chen, J. C. Fast Drop Movements Resulting from the Phase Change on a Gradient Surface. *Science* **2001**, *291*, 633−636.

(11) Macner, A. M.; Daniel, S.; Steen, P. H. Condensation on Surface Energy Gradient Shifts Drop Size Distribution toward Small Drops. *Langmuir* **2014**, *30*, 1788−1798.

(12) Razzaghi, A.; Banitabaei, S. A.; Amirfazli, A. Shedding of Multiple Sessile Droplets by an Airflow. *Phys. Fluids* **2018**, *30*, No. 087104.

(13) Antonini, C.; Carmona, F. J.; Pierce, E.; Marengo, M.; Amirfazli, A. General Methodology for Evaluating the Adhesion Force of Drops and Bubbles on Solid Surfaces. *Langmuir* **2009**, *25*, 6143−6154.

(14) Barghi, F.; Entezari, M.; Chini, S. F.; Amirfazli, A. Effect of Initial Wetting State on Plastron Recovery through Heating. *Int. J. Heat Mass Transfer* **2020**, *156*, No. 119705.

(15) Papakonstantinou, C. A.; Chen, H.; Bertola, V.; Amirfazli, A. Effect of Condensation on Surface Contact Angle. *Colloids Surf., A* **2022**, *632*, No. 127739.

(16) Madani, S.; Amirfazli, A. Oil Drop Shedding from Solid Substrates by a Shearing Liquid. *Colloids Surf., A* **2014**, *441*, 796−806.

(17) Moghtadernejad, S.; Tembely, M.; Jadidi, M.; Esmail, N.; Dolatabadi, A. Shear Driven Droplet Shedding and Coalescence on a Superhydrophobic Surface. *Phys. Fluids* **2015**, *27*, No. 032106.
(18) Karmali, F.; Shelhamer, M. The Dynamics of Parabolic Flight: Flight Characteristics and Passenger Percepts. *Acta Astronaut.* **2008**, *63*, 594−602.
(19) Brutin, D.; Zhu, Z.; Rahli, O.; Xie, J.; Liu, Q.; Tadrist, L. Sessile Drop in Microgravity: Creation, Contact Angle and Interface. *Microgravity Sci. Technol.* **2009**, *21*, 67−76.
(20) Diana, A.; Castillo, M.; Brutin, D.; Steinberg, T. Sessile Drop Wettability in Normal and Reduced Gravity. *Microgravity Sci. Technol.* **2012**, *24*, 195−202.
(21) Milne, A. J. B.; Amirfazli, A. Drop Shedding by Shear Flow for Hydrophilic to Superhydrophobic Surfaces. *Langmuir* **2009**, *25*, 14155−14164.
(22) Mandal, D. K.; Criscione, A.; Tropea, C.; Amirfazli, A. Shedding of Water Drops from a Surface under Icing Conditions. *Langmuir* **2015**, *31*, 9340−9347.
(23) Roisman, I. V.; Criscione, A.; Tropea, C.; Mandal, D. K.; Amirfazli, A. Dislodging a Sessile Drop by a High-Reynolds-Number Shear Flow at Subfreezing Temperatures. *Phys. Rev. E* **2015**, *92*, No. 023007.
(24) Mehta, R. D.; Bradshaw, P. Design Rules for Small Low Speed Wind Tunnels. *Aeronaut. J.* **1979**, *83*, 443−453.
(25) Shakeri Bonab, M.; Kempers, R.; Amirfazli, A. Determining Transient Heat Transfer Coefficient for Dropwise Condensation in the Presence of an Air Flow. *Int. J. Heat Mass Transfer* **2021**, *173*, No. 121278.
(26) Sugioka, K. I.; Komori, S. Drag and Lift Forces Acting on a Spherical Water Droplet in Homogeneous Linear Shear Air Flow. *J. Fluid Mech.* **2007**, *570*, 155−175.
(27) Kolinski, J. M.; Mahadevan, L.; Rubinstein, S. M. Lift-Off Instability During the Impact of a Drop on a Solid Surface. *Phys. Rev. Lett.* **2014**, *112*, 1−5.
(28) Shakeri Bonab, M.Investigation of Heat Transfer in Dropwise Condensation Facilitated by a Humid Airflow. Doctoral Dissertation, York University: Toronto, Canada, 2022.

https://doi.org/10.1021/acs.langmuir.2c01898
Langmuir 2023, 39, 64−74